



## Measurement of the inductance of resistive magnets: two case studies

M. Buzio, R Chritin, D. Giloteaux / TE-MSC

Keywords: non-linear inductor, differential inductance, apparent inductance, fixed-coil magnetic measurement, PS MTE octupole, SPS main dipole

---

---

### Summary

This note concerns the main definitions of self-inductance (i.e. differential, secant and energy-based) that are relevant for the electromagnetic modelling of accelerator magnets. In particular, we consider the case of iron-dominated resistive magnets. The different definitions, which coincide in the linear limit at low field, tend to diverge dramatically as the iron becomes saturated. We describe the measurement technique and the results for two case studies, i.e. the PS MTE octupole and a main SPS dipole of MBB type. We show that the differential inductance may drop dramatically at high current, up to about a factor two, even for magnets where the field non linearity is within a few percent only.

---

### 1. Introduction

Accelerator magnets can store large amounts of magnetic energy, mostly concentrated in the aperture, and thus behave electrically like very large inductors with typical values ranging from a few to a few hundred millihenry. The energy stored in dipole magnets is usually much higher than in multipoles of comparable size and peak field strength, owing to the uniform field distribution; however, the self-inductance is proportional to the square of the number of excitation coil turns and is therefore strongly dependent upon the specific design of each magnet.

Accurate knowledge of the load represented by a magnet for the power converter is essential for precise and stable control of the field produced, especially for fast-cycled magnets where the inductive voltage represents the major component. For typical resistive (normal conducting) magnets the inductance will be dominated by the presence of the iron core, which leads to non-linearity mainly in the form of saturation (lower field/current ratio at high current) and hysteresis (increased field for the same current on a ramp down with respect to a ramp up). Hysteresis effects are usually small (of the order of  $10^{-3}$  of the nominal field) and rarely relevant, except for specific situations e.g. in machines with large pulse-to-pulse modulation, or when the beam is present on both ramp directions. On the other hand, saturation often affects dramatically the inductance and hence final performance.

The present note is concerned with the experimental evaluation of the inductance  $L(I)$  of resistive magnets as a function of the excitation current level, within a target uncertainty of the order of 1% (similar considerations apply in principle also to superconducting magnets, for which saturation effects are typically at least one order of magnitude smaller). The main aim is to establish the drop  $\Delta L$  that has to be expected due to saturation at high current (Fig. 1). We shall see that several definitions of the inductance are possible, which all coincide in the linear case and diverge at high field when saturation occurs. Many different definitions are covered in the existing literature, which however concerns mostly inductors without air gaps (see e.g. [1]) and rotating machines, which are dominated by various types of losses. If the magnet cycle period is long (1~1000 s), as is often the case for CERN accelerators, the effects of losses due to hysteresis and eddy currents are small and will be ignored in this note.

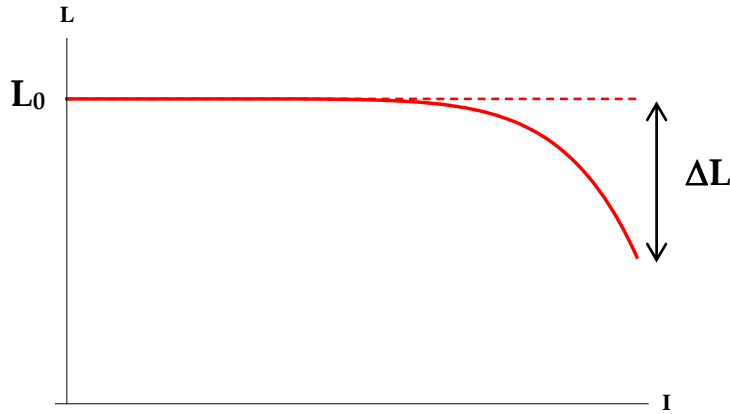


Fig. 1 – General qualitative behavior of magnet inductance  $L$  vs. excitation current  $I$

## 2. Theoretical aspects

### 2.1 Simplified electromagnetic model

A typical resistive magnet can be represented ideally by an excitation coil with  $N_t$  turns producing the magnetic flux  $\Phi$ , plus an iron yoke with relative permeability  $\mu_r$  that channels the flux to an air gap where a useful magnetic field is produced. In the 2D case (i.e. infinitely long magnet), represented schematically in Fig. 2, the field in the gap  $g$  is given by:

$$B = \frac{\mu_0 \mu_r N_t I}{\ell + \mu_r g} \quad (1)$$

where  $\ell$  represents the average length of the magnetic circuit within the iron. The field is commonly measured with a pick-up coil via integration of the induced voltage  $V_{coil}$ . In reality, some of the flux will leak out of the iron, short-circuiting the gap, passing in part through the coil itself. The amount of leakage flux depends upon the overall field level and the geometry, since saturation is reached at different excitation levels in different parts (e.g. sharp edges concentrate the field and saturate much sooner than the bulk).

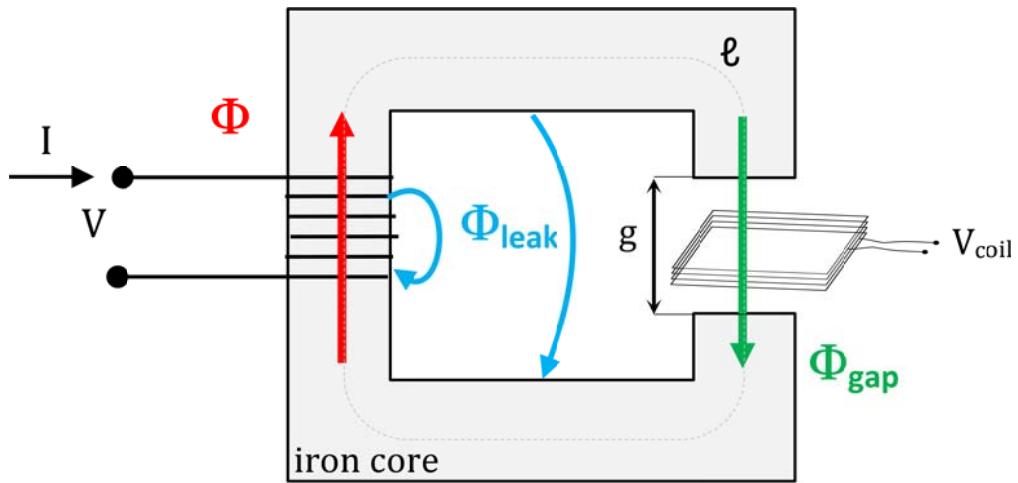


Fig. 2 – Schematic representation of a resistive dipole magnet

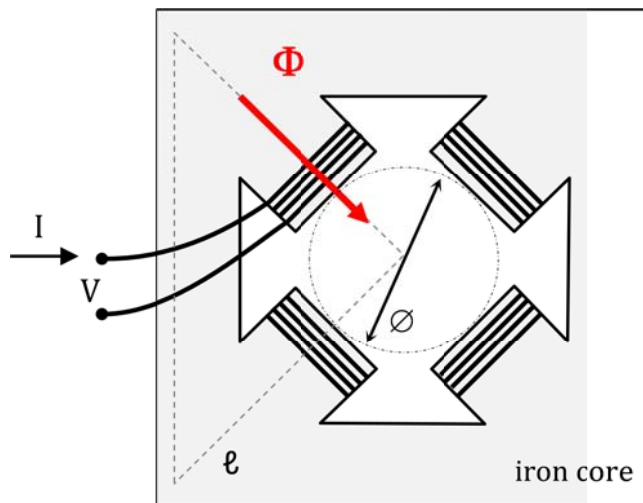


Fig. 3 – Schematic representation of a resistive quadrupole magnet  
(the four coils are in series with alternating polarities)

Analogous considerations for a quadrupole magnet lead to the following simplified expression for the field gradient in the gap, assumed to be round with diameter  $\emptyset$ :

$$G = \frac{8\mu_0\mu_r N_p I}{(2\ell + \mu_r \emptyset)\emptyset} \quad (2)$$

where  $N_p$  is the number of turns per pole and  $\ell$  is the average length of one of the four symmetric magnetic circuits in the iron (Fig. 3).

## 2.2 Definition of inductance based on magnetic flux

The **apparent** or **secant inductance**  $L$  of the excitation coil is defined as the ratio of the excitation current  $I$  to the *total* flux  $\Phi$  linked through the coil itself (see [2], §33):

$$L \equiv \frac{\Phi}{I} \quad (3)$$

Assuming that all  $N_t$  turns in series generate the same flux  $\Phi_t$ , the total flux generated can be expressed by:

$$\Phi_{gen} = N_t \Phi_t = N_t L_t I \quad (4)$$

where  $L_t$  represents the self-inductance of a single turn. Taking flux leakage into account, the total flux  $\Phi$  linked through the excitation coil is given by:

$$\Phi = N_t \Phi_{gen} (1 - \lambda_{coil}) \quad (5)$$

where  $\lambda_{coil}$  represents the fraction that is *not* linked back into the excitation coil. The self-inductance (3) can be therefore written as:

$$L = N_t \frac{\Phi_{gen}}{I} (1 - \lambda_{coil}) = N_t^2 (1 - \lambda_{coil}) L_t \quad (6)$$

which shows explicitly the well-known dependence upon the square of the number of turns.

### 2.2.1 Relationship between apparent inductance and magnetic field

Due to leakage, the magnetic flux in the gap  $\Phi_{gap}$  will be in general a fraction of the total flux generated. Taking for simplicity the case of a dipole, where the flux in the gap is given by the field  $B$  passing through the pole surface  $A$ , we can write:

$$\Phi_{gap} = \Phi_{gen} (1 - \lambda_{yoke}) = BA \quad (7)$$

where  $\lambda_{yoke}$  represents the fringe field that short-circuits the gap. Substituting  $\Phi_{gen}$  derived from (7) in (6), we find that:

$$L = N_t A \frac{B}{I} \frac{1 - \lambda_{coil}}{1 - \lambda_{yoke}} \quad (8)$$

From (8) we see that leakage from the coil always reduces the inductance, while leakage from the yoke, *for a given flux in the gap*, increases the inductance. In the linear regime, normally approximated by the behavior at low field, the transfer function  $B/I$  and the leaked flux fractions are constant so that also the inductance is constant i.e.  $L=L_0$ . In reality  $B$ ,  $\lambda_{coil}$  and  $\lambda_{yoke}$  are non-linear functions of the current  $I$ , and by differentiating (8) w.r.t.  $I$ , dividing the resulting expression by (8) and assuming further that  $\lambda_{yoke}, \lambda_{coil} \ll 1$  we find that:

$$\frac{\Delta L}{L} \approx \frac{\Delta B}{B} - \Delta \lambda_{coil} + \Delta \lambda_{yoke} \quad (9)$$

Equation (9) clarifies how different sources of non-linearity affect the inductance. The first term  $\Delta B/B$  is mainly linked to the material's properties, i.e. the magnetic permeability curve, while the non-linearities of the leakage fractions are mainly a function of the geometry. For instance, if we assume an infinitesimally thin excitation coil then  $\lambda_{coil}=0$ , while if we take e.g. a toroidal yoke geometry with very large aspect ratio then  $\lambda_{yoke}=0$ . In general, however, the leakage fractions are small (a few %) and the inductance drop due to saturation is of the same order as the drop of the magnetic field. We may consider two extreme cases, depending on the ratio between the magnetic length  $l_m$  and the gap size:

- short magnet ( $l_m/g \approx 1$ ): as the iron saturates, a large fraction of the total flux tends to leak at the ends and through the coils, so that in (9)  $\Delta \lambda_{coil}$  becomes the dominant term and therefore:

$$\frac{\Delta L}{L} \lesssim \frac{\Delta B}{B} \quad (10)$$

- long magnet ( $l_m/g \gg 1$ ): as the iron saturates, a large fraction of the total flux tends to leak from the yoke, so that in (9)  $\Delta \lambda_{yoke}$  becomes the dominant term and therefore:

$$\frac{\Delta L}{L} \gtrsim \frac{\Delta B}{B} \quad (11)$$

The two case studies that follow provide examples of these two extremes.

### 2.3 Definition of inductance based on circuit behaviour

From the point of view of the electrical circuit powering the magnet, one can express the voltage drop at the magnet leads as the sum of a resistive and an inductive component  $d\Phi/dI$  obtained by differentiating (3):

$$V = RI + \frac{d\Phi}{dt} = RI + \frac{d}{dt}(LI) \quad (12)$$

The so-called **differential inductance**  $L_d$  (a.k.a *incremental* inductance) is defined as the incremental ratio of flux to current or, equivalently, as the ratio of the inductive voltage to the current ramp rate [3]:

$$L_d \equiv \frac{d\Phi}{dI} = \frac{V - RI}{\frac{dI}{dt}} \quad (13)$$

Using this definition, the equivalent circuit equation can be written more simply:

$$V = RI + L_d \frac{dI}{dt} \quad (14)$$

From (13), we see that the differential inductance  $L_d(I)$  can be related to  $L(I)$  via the following linear differential equation:

$$L_d = L + I \frac{dL}{dI} \quad (15)$$

Assuming the initial condition  $L_d(0) = L(0) = L_0$ , integration of (15) provides the link between the two definitions. Since in all practical cases  $dL/dI < 0$ , the differential inductance is always lower than the apparent inductance. The difference tends to vanish in the linear regime, i.e. when either  $I \rightarrow 0$  or  $I \rightarrow \infty$  (complete saturation), and will be maximum in the current range corresponding to both high  $dL/dI$  and high current.

From (15), we can infer that the effects of saturation in  $L_d(I)$  are at least as large as the effects in  $L(I)$ , plus an additional term  $IdL/dI < 0$  that depends on the shape of the  $L(I)$  curve and that grows larger at higher currents. Qualitatively, we can therefore predict that the **drop of the differential inductance due to saturation will be high in magnets where the transition to saturation occurs sharply and at high current**. For instance, this is the case for a well-optimized magnet, with no field concentrations and a uniform distribution of field within the iron. By contrast, magnets having an insufficient volume of iron in the yoke and/or sharp edges<sup>1</sup> will experience an earlier onset of saturation and a smoother transition, resulting in lower  $\Delta L_d$ .

## 2.4 Definition of inductance based on magnetic energy

The inductance can be directly related to the energy  $W$  stored in the magnetic field, which provides in principle a definition suitable for computation via (21) in those cases when the field is known throughout the whole volume occupied, e.g. from a standard finite element simulation. The stored energy can be calculated as a function of the time by integrating the electrical input power  $V(t)I(t)$ , taking into account only the inductive voltage component (i.e. neglecting the dissipative term in  $R$ ), making use of (12):

$$W(t) = \int_0^t (V - RI)Idt' = \int_0^t I \frac{d}{dt'} (LI)dt' = \int_0^\Phi Id\Phi' \quad (16)$$

Integrating by parts, we may express the energy as a function of the current  $I$ :

$$W(I) = LI^2 - \int_0^I L(I')I'dI' = I\Phi - \int_0^\Phi \Phi dI' \quad (17)$$

Equation (17) can be represented graphically in the  $(I, \Phi)$  plane as shown in Fig. 4, where we can see that the energy  $W$  is given by the area between the  $\Phi=LI$  curve and the  $\Phi$  axis, while the area  $W^*$  between the curve and the  $I$  axis is also known as the magnetic coenergy [4]. In the linear case, i.e. when  $L$  is a constant, (17) yields the well-known relation  $W = \frac{1}{2}LI^2$ . By analogy, in the general case we can define an **energy-equivalent inductance  $L_w$**  such that:

$$W \equiv \frac{1}{2}L_w I^2 \quad (18)$$

---

<sup>1</sup> This is often true for very short or small magnets, where the amount of iron close to edges and hence concentrating the field is higher w.r.t. the total volume of the yoke.

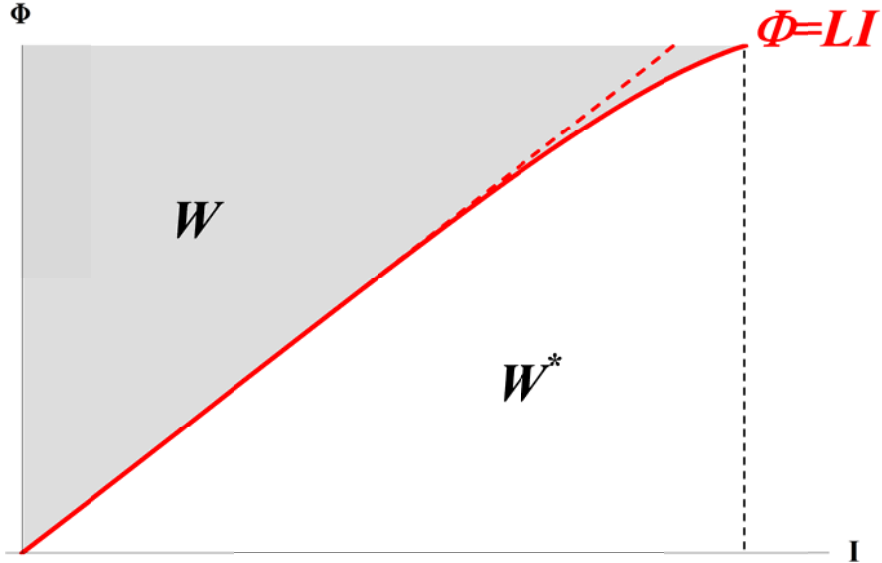


Fig. 4 – General  $\Phi/I$  relationship, where  $\Phi=LI$ . The shaded area represents the magnetic energy  $W$ .

The relationship between  $L_w$  and  $L$  can be derived by equating (16) to (18) and integrating once more by parts:

$$L_w = L + \frac{1}{2I^2} \int_0^I I^2 dL' \quad (19)$$

We see that  $dL \leq 0$  implies that  $L_w \leq L$ . In practice, the dynamic inductance can be readily evaluated from electrical measurements of  $V(t)$  and  $I(t)$ :

$$L_w = \frac{2}{I^2} \int_0^t (V - RI) Idt' \quad (20)$$

These measurements are very often easily available directly from the converter powering the magnet. The energy actually stored in the inductor could also be obtained, in principle, from integration of the magnetic energy density over the whole volume  $\mathbb{V}$ :

$$W = \iiint_{\mathbb{V}} \frac{B^2}{2\mu} d\mathcal{V} \quad (21)$$

The rigorous evaluation of (21), however, is quite impractical whichever way one may choose to do it, based either on simulations or measurements<sup>2</sup>. On the other hand, it is useful to relate the energy-equivalent inductance to the magnetic field by equating (18) to (21), so as to obtain:

$$L_w(I) = \iiint_{\mathbb{V}} \frac{1}{\mu} \left( \frac{B(I)}{I} \right)^2 d\mathcal{V} \quad (22)$$

---

<sup>2</sup> The reasons are different in the two cases: a computer simulation must represent the 3D geometry in full detail, which makes it computationally expensive, and its accuracy will be affected by the relatively low precision with which the magnetic properties of the iron are usually known as a function of the position and of the other parameters; an experimental approach, based for example on integration of the Maxwell stress tensor around a closed surface enclosing the volume of interest, requires on the other hand an extremely detailed mapping which may be practically very difficult to achieve.

where  $B/I$  represents the field transfer function of the magnet, which is variable from point to point and as a function of the current. From a qualitative viewpoint, by averaging the integrand and differentiating on both sides of (22) we obtain:

$$\frac{\Delta L_w}{L_w} \approx 2 \frac{\Delta(B/I)}{B/I} = 2 \frac{\Delta B}{B} \quad (23)$$

(taking also into account that the relative non-linearity of the field is the same as the non-linearity of the transfer function). By comparing (9) to (23) we conclude that the **relative drop of dynamic inductance due to saturation is approximately twice as big as the drop of the apparent inductance**.

### 2.3.1 Partial inductance due to the energy in the air gap

At first approximation it may be useful to carry out the integral in (21) only over the air gap of the magnet, which normally represents the dominant contribution due to the combination of high field and low permeability ( $\mu = \mu_0$ ). Let us consider for instance a dipole with a rectangular air gap  $g$  of effective width  $a$  and a quadrupole with a round gap of diameter  $\emptyset$ . If the magnetic length in both cases is  $l_m$ , we can express the corresponding values of the **gap inductance  $L_g$**  as:

$$\text{dipole} \quad L_g = \frac{1}{\mu_0} \left( \frac{B}{I} \right)^2 g a l_m \quad (24)$$

$$\text{quadrupole} \quad L_g = \frac{\pi}{16\mu_0} \left( \frac{G}{I} \right)^2 \emptyset^4 l_m \quad (25)$$

where  $B/I$  and  $G/I$  represent the respective average transfer functions. With the aim of deriving rough but very simple approximate expression based only on the geometry of the magnet, it is possible to estimate field and gradient from (1) and (2) respectively in the limits  $\ell \ll \mu_0 g$ ,  $\ell \ll \mu_0 \emptyset$  to obtain:

$$\text{dipole} \quad L_g = \mu_0 N_t^2 \frac{a}{g} l_m \quad (26)$$

$$\text{quadrupole} \quad L_g = 8\pi\mu_0 N_p^2 l_m \quad (27)$$

We remark that, for magnet gaps of unit aspect ratio (i.e. round or square), the partial inductance does not depend at all on the size of the gap but only on the magnet length and the number of excitation coil turns.

## 2.4 Relationship between $L$ , $L_d$ and $L_w$

The link between the different definitions of inductance can be better clarified by taking, as an example, a simple expression for  $L(I)$  in closed form. We shall hereafter consider the following model:

$$L(I) = L_0 \left( 1 - \left( \frac{I}{I^*} \right)^n \right) \quad (28)$$

where the current  $I^*$  and the exponent  $n$  are fitting parameters. For values of  $n$  sufficiently high this expression has been found to fit experimental data reasonably well; in particular, it provides an almost flat curve for  $I \rightarrow 0$ , and a drop to 0 for  $I \rightarrow I^*$  which becomes sharper as  $n$  increases.

By substitution of (28) in (13) and (17), the corresponding expressions for the differential and dynamic inductance can be readily found (see an example plot in Fig. 5):

$$L_d(I) = L_0 \left( 1 - (1+n) \left( \frac{I}{I^*} \right)^n \right) \quad (29)$$

$$L_w(I) = L_0 \left( 1 - 2 \frac{1+n}{2+n} \left( \frac{I}{I^*} \right)^n \right) \quad (30)$$

From (28), (29) and (30) we can evaluate the magnitude of the drop due to saturation in the differential and energy-equivalent inductance *relative* to the apparent inductance:

$$\frac{\Delta L_d}{\Delta L} = 1 + n \quad (31)$$

$$\frac{\Delta L_w}{\Delta L} = 2 \frac{1+n}{2+n} \quad (32)$$

We observe that the effects of saturation in  $L_d(I)$  and  $L_w(I)$  are always proportional to the effect in  $L(I)$ , irrespective of the current. In addition, we see that for increasing values of the exponent  $n$  (which describe magnets with delayed, but sharper saturation) the drop of energy equivalent inductance tends to a limit magnitude  $\Delta L_w \rightarrow 2\Delta L$  (consistently with (23)), while the drop of the differential inductance grows unbounded.

In other words, this confirms that the **divergence between differential and apparent inductance grows larger for magnets which exhibit sharper saturation at higher current**. This explains the large variations in differential inductance that may be observed at high current even on apparently well-behaved magnets (i.e. magnet which exhibit linear behavior up to high current).

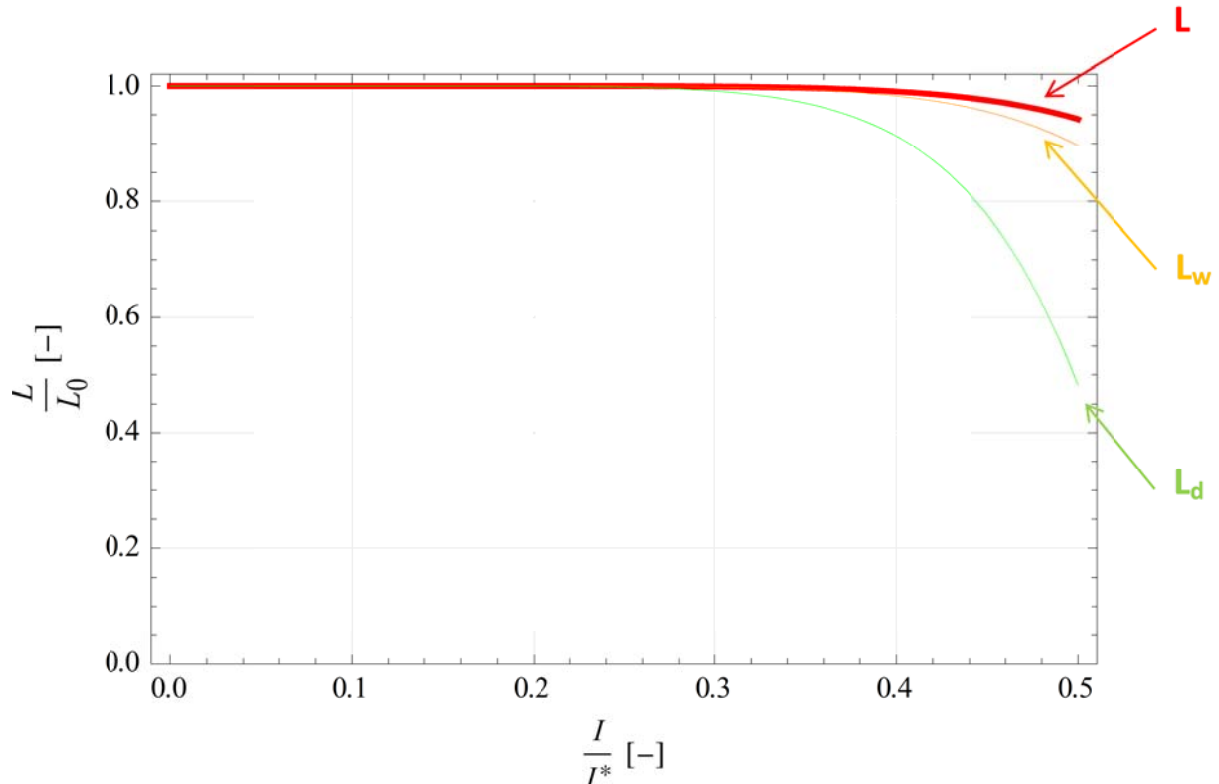


Fig. 5 – Examples of simulated  $L(I)$ ,  $L_d(I)$  and  $L_w(I)$  curves for  $n=10$   
(to be compared to Fig. 13)

### 3 Measurement procedure

All the above defined versions of the inductance can be derived from a continuous measurement of the waveforms of excitation current  $I(t)$  and voltage  $V(t)$ , which have to be acquired with an ADC with a time resolution  $\Delta t$  sufficient to provide the desired resolution  $\Delta L$ . The differential and energy equivalent inductances can be obtained directly from (15) and (20) respectively, while the apparent inductance  $L(I)$  can be computed as detailed below (§3.2 and 3.3). The results thus obtained are valid in the quasi-static limit, i.e. for  $f \rightarrow 0$ . Since standard electronic inductance measurements are normally carried out with an AC bridge with very small currents and typical frequencies of 50 Hz and above, direct comparison between these results is not always accurate.

#### 3.1 Test setup

The measurements reported below (§5) have been carried out with a multiplexed 16-bit ADC, National Instruments USB 6216. This kind of device is sometimes affected by cross-talk between channels or small voltage offsets which may, especially for long acquisition times, affect the accuracy of the integrated voltages; in this case, an error of about 0.8 mV on the  $V_{coil}$  channel had to be corrected.

The time resolution needed may be estimated assuming, for simplicity, a linear drop from  $L_0$  to zero over the current range from  $I(0)=0$  to  $I=I_{max}$ . Since:

$$\frac{dL}{dt} = \frac{dL}{dI} I \quad (33)$$

the upper limit of the sampling time is given by:

$$\Delta t \leq \frac{\Delta L}{L_0} \frac{I_{max}}{\dot{I}} \quad (34)$$

In the case study II below, a sampling frequency of 20 kHz was used. The current was read via a Hazemayer DCCT with a sensitivity ratio of 600 A/V. The voltage drop at the excitation coil was read through connectors fixed onto the main current leads, in order to improve the accuracy of the resistance measurement, using a  $10\times$  voltage divider.

### 3.2 Integration in the time domain

Equation (12) can be integrated in the time domain starting from an arbitrary  $I_0=I(0)$  to obtain:

$$LI - L_0 I_0 = \varphi(t) = \int_0^t (V - RI) dt' \quad (35)$$

If  $I_0$  is sufficiently low, the initial value of the inductance  $L_0$  can be taken from any other available measurement. Assuming that the function  $I(t)$  can be inverted to obtain uniquely  $t(I)$ , the result can be expressed as a function of the current:

$$L(I) = L_0 \frac{I_0}{I} + \frac{\psi(I)}{I} \quad (36)$$

where  $\psi(I)=\varphi(t(I))$ , with  $\psi(I_0)=0$ . This method, as we shall see in the examples below, provides smooth results thanks to the integration that filters away unwanted measurement noise. Numerical difficulties may arise when  $I_0 \approx 0$ , in the limit for  $I \rightarrow 0$  when the ratio  $\psi(I)/I$  becomes indeterminate and may fail to yield a stable value  $L_0$ .

The differential inductance  $L_d$  can then be computed equivalently either from the definition (13) or from (15). In both cases, the accuracy of the result is impaired by the numerical differentiation, which unavoidably entails a certain amount of noise.

### 3.3 Integration in the current domain

As an alternative, if the function  $L_d(I)$  is already known (e.g. from existing measurements) one may consider direct integration of (15). A closed-form solution exists (see e.g. [5], §1.1.34) and it can be written as:

$$L(I) = L_0 \frac{I_0}{I} + \frac{1}{I} \int_{I_0}^I L_d dI' \quad (37)$$

whereby we find that  $\psi(I) = \int_{I_0}^I L_d dI'$ . The result is, of course, exactly the same as (36).

## 4 Case study I: PS MTE octupole

In January 2011 a discrepancy was remarked between the saturation effects on the main field of the PS Multi Turn Extraction octupoles, i.e. **4.9%** at 550 A according to a recent test campaign (Fig. 6), and a much larger differential inductance variation up to about 60% at 650 A seen by the power converter (Fig. 7).

On the basis of the measured  $L_d(I)$  and  $I(t)$ , the inductance  $L(I)$  was calculated and the result is plotted in Fig. 7. The  $L_d(I)$  curve is well fitted by (29) taking  $I^*=1030$  A and  $n=5$ , which gives the opportunity to interpolate between the 7 data points available. The apparent inductance  $L(I)$  can be computed from (28) or (37).

The drop of  $L(I)$  due to saturation at 550 A is found to be **4.2%**, quite close to the drop of the field. The difference is consistent with (10) in the case  $\lambda_{coil} > \lambda_{yoke}$ , corresponding to a magnet with very low length/gap aspect ratio (which for a MTE octupole is about 0.3). The additional fringe field fraction at 550 A can be estimated in this case to be  $\Delta\lambda_{coil} \geq 0.7\%$ .

The interpolated drop of  $L_d(I)$  at 550 A is about **26%**, which is roughly consistent with (25) with some allowance for the approximation due to the limited number of data points.

To conclude, the **large drop of the differential induction at high current and the relatively small saturation measured of the main field are consistent** within the framework of the present model.

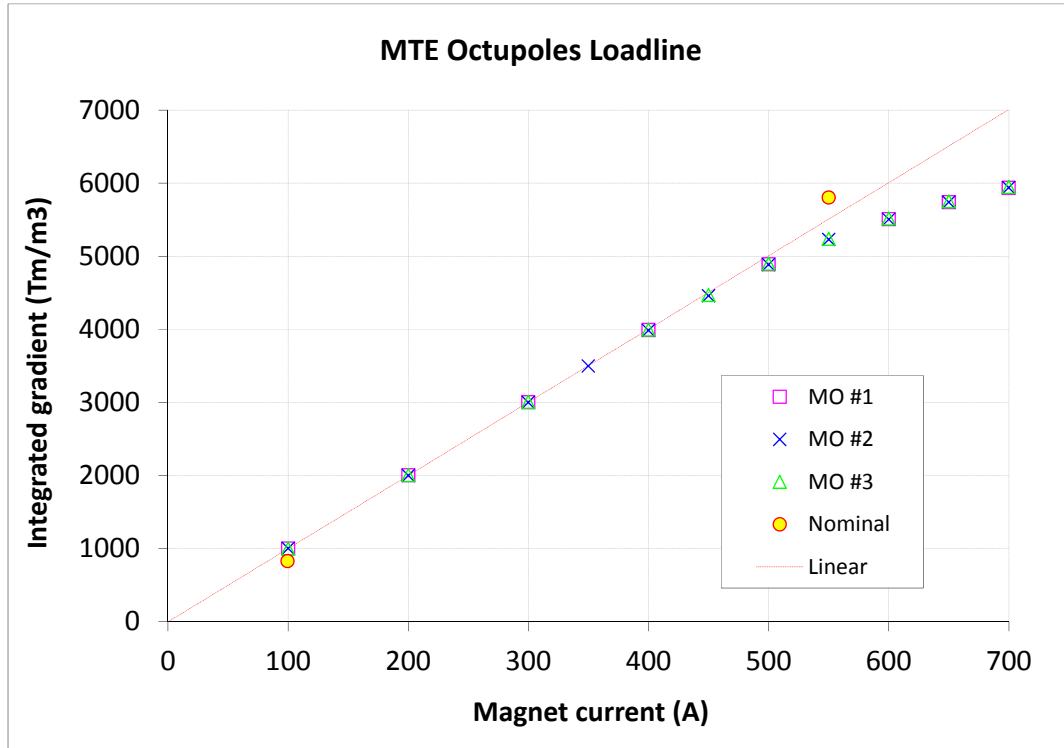


Fig. 6 – Integral magnetization curve of MTE octupoles

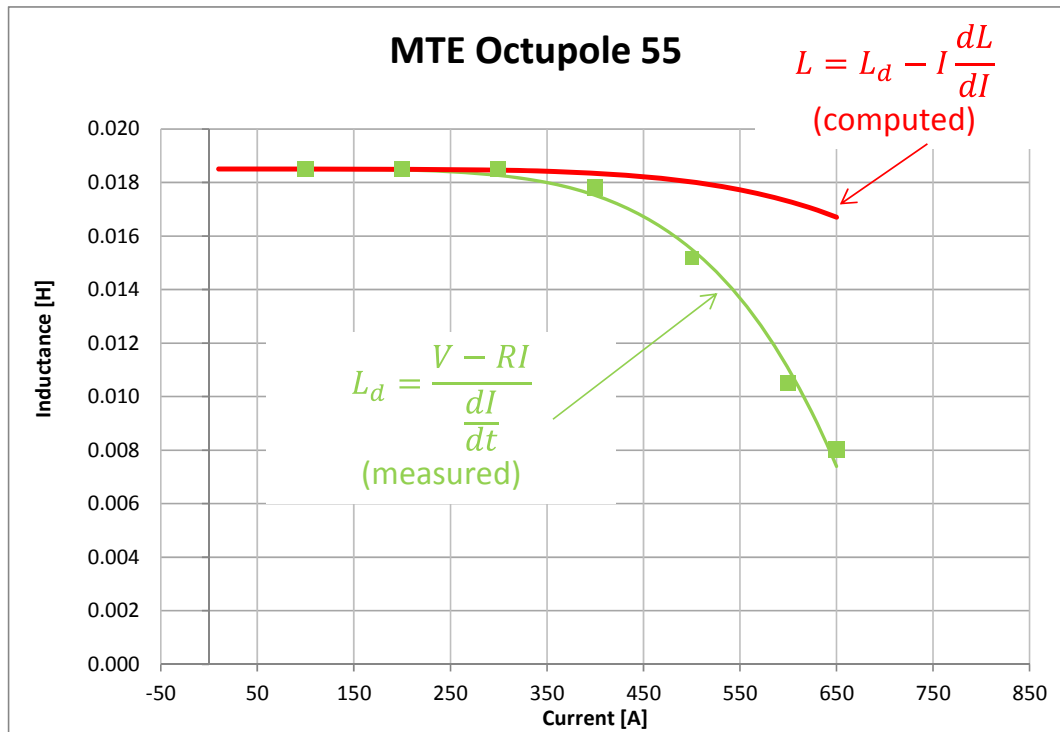


Fig. 7 – Differential (measured) and apparent (calculated) inductance of a PS MTE octupole  
(original data  $L_d(I)$  courtesy of G. le Godec)

## 5 Case study II: main SPS dipole type MBB

The main SPS dipole MBB 004, used since the construction of the machine as an integral field reference in the test station in bldg. 867, was measured in May 2011. The main goal of the test was to verify the value of the inductance at high field as needed to improve the stability of the current control during operation.

The test was carried out using a standard measurement current cycle, which is slightly different from actual machine cycles (max. field equal to 1.8 rather than 2.05 T, same cycle for MBA and MBB types). In addition to  $V(t)$  and  $I(t)$ , also the voltage  $V_{coil}(t)$  induced on an integral pick-up coil inserted into the magnet was taken in order to estimate the magnetic field energy in the gap.

The raw measurements are plotted in Fig. 8. The small voltage glitch visible on both coil signals at  $t \approx 4.6$  s is due to a step in the excitation current, as one can more clearly see in Fig. 9. This feature does not alter in any way the results of this test.

### 5.1 Magnetization curve and transfer function

The integral magnetization curve  $BdL(I)$  obtained from the integration of  $V_{coil}(t)$  is plotted in Fig. 10, while the transfer function i.e. the ratio  $BdL/I$  is plotted in Fig. 11. Saturation can be seen to set in around 4000 A (although the magnetization curve is not perfectly linear even below this threshold), and the drop on the flat-top at 4900 A is  $\Delta B/B = 3.4\%$ . The sharp rise of the transfer function below about 500 A is due to the presence of a residual field, which can be estimated from the offset of the magnetization curve to be on average about **36 G** i.e.  $2 \cdot 10^{-3}$  of the peak field. In relative terms, the width of the hysteresis cycle peaks at about **1.2%** at low field.

### 5.2 Eddy current effects

The effects of the eddy currents have been measured in order to identify the DC segment of the flat top where to carry out coil resistance measurement (see §5.3 below). The lag of the field w.r.t. excitation current has been calculated by first scaling the integrated field to match the current  $I(4.5)$  at the end of the flat-top, subtracting  $I(t)$  and then normalizing to  $I(4.5)$ . The resulting relative field error curve, plotted in red in Fig. 12, shows an exponential decay with amplitude about  $4 \cdot 10^{-4}$  and time constant  $\tau \approx 100$  ms, meaning that perturbations can be considered to vanish effectively 300 ms after the end of the ramp.

### 5.3 Coil resistance and temperature effects

The coil resistance  $R$  has been checked by taking the average of the V/I ratio on the flat-top (see Fig. 13), where both inductive voltages and eddy currents effects are negligible. A priori either a current flat-top or flat bottom might have been used, however the magnified curve plotted in orange in Fig. 13 shows clearly that flat-bottom measurements are far too noisy to be reliable. The average on the flat-top provides a value  **$R=4.552$  mΩ** at 20°C, in good agreement with the nominal value of 4.42 mΩ obtained at  $I \approx 0$  with a standard four-wire technique.

The measurement has been repeated after cycling continuously the magnet in order to simulate the thermal conditions of the machine in operation. After 90 min. of cycling the

resistance had increased to 4.60 mΩ, corresponding to an average ΔT of 3.4°C. No further increase has been observed after an additional period of 90 min, suggesting that thermal conditions had already reached a steady state. The observed ΔT is much lower than what is experienced in operation (estimated about 15 °C), probably due to a combination of lower duty cycle and higher water flow rate on the test bench. Anyway, repeating the inductance measurements after 90 and 180 min. gives essentially the same results, in accord with the fact that the temperature is not expected to affect the measurement.

#### 5.4 Inductance measurements

The four versions of the inductance discussed above, i.e.  $L$ ,  $L_d$ ,  $L_w$  and  $L_g$  have been computed from (35), (13), (20) and (24) respectively and the results are plotted in Fig. 14.

At a first glance, we remark that the measurement of the differential inductance  $L_d(I)$  is strongly affected by the noise due to the  $dI/dt$  derivative. On the top and bottom plateaux  $dI/dt \approx 0$  and as a result the computed  $L_d$  tends to diverge, as the numerator of (13) is affected by measurement errors and fluctuates around zero. By contrast, the measurements of the apparent and energy equivalent inductance are smoothed by the integration and appear to provide a more precise result.

The curves  $L(I)$  and  $L_w(I)$  are extremely sensitive upon the value of  $R$  used in the calculation. For instance, a variation of  $R$  of  $10^{-4}$  (i.e. just 0.4 μΩ) provokes about 10% error in the low current region  $I < 1000$  A, where large hysteresis-like artifacts are evident. These are due to cancellation errors in the term  $(V - RI)$  appearing in (35) and (20), combined with the amplification provided by the factor  $1/I$ . The inductance should be expected to exhibit a certain amount of hysteresis, which may be estimated to be around 1% by comparison with the magnetization curve; however, the artifacts visible at low current in Fig. 14 are far too large and should be considered measurement errors.

In the region between 1000 and 3500 A, the curves  $L(I)$ ,  $L_w(I)$  and  $L_d(I)$  coincide within a few  $10^{-3}$  ( $L_d$  must of course be averaged) to the value  $L_0 = 9.85$  mH, very close to the nominal value of 9.9 mH measured with a standard AC bridge at  $I \approx 0$ . Such good agreement occurs irrespective of the precise value taken for  $R$ , which supports the overall robustness of the procedure.

The inductance  $L_g$  calculated on the basis of the energy in the air gap, on the other hand, has been estimated very roughly from (24) taking the field to be uniform over a volume  $gal_m = 52 \times 240 \times 6300$  mm<sup>3</sup>. The result is about 10% lower than  $L_w$  at high current, but the estimation falls dramatically short at low current and therefore is not useful in practice.

### 5.4.1 Inductance drop due to saturation

The drop due to saturation of the apparent inductance curve  $L(I)$ , calculated at 4900 A, is  $\Delta L/L_0 \approx 4\%$ , slightly larger than the drop of the magnetization in agreement with (11) for the case of a magnet with a high aspect ratio ( $\sim 120$ ). The additional fraction of flux leaking from the yoke can be estimated in this case to be  $\Delta\lambda_{yoke} \geq 0.6\%$ .

The drop of the differential and energy equivalent inductance is respectively:

$$\frac{\Delta L_d}{L_0} \approx 39.4\% \quad \frac{\Delta L_d}{\Delta L} \approx 10$$

$$\frac{\Delta L_w}{L_0} \approx 7.2\% \quad \frac{\Delta L_w}{\Delta L} \approx 1.8$$

This is in very good agreement with (31) and (32), and consistently with the curve  $L(I)$  being nicely fitted by (22) with  $n=9$ ,  $I^*=12$  kA.

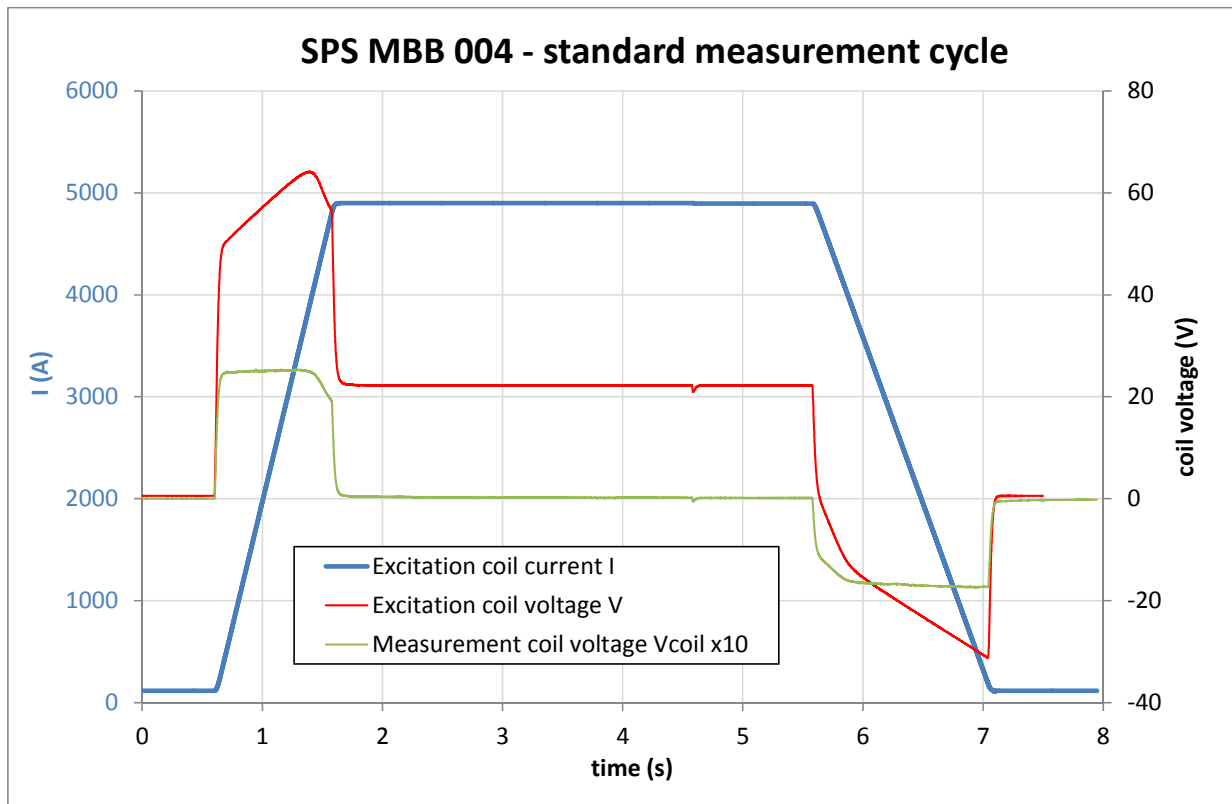


Fig. 8 – Signals measured at 20 kHz during a SPS reference MBB current cycle.  
The green curve ( $V_{coil}$ ) has been magnified by a factor 10.

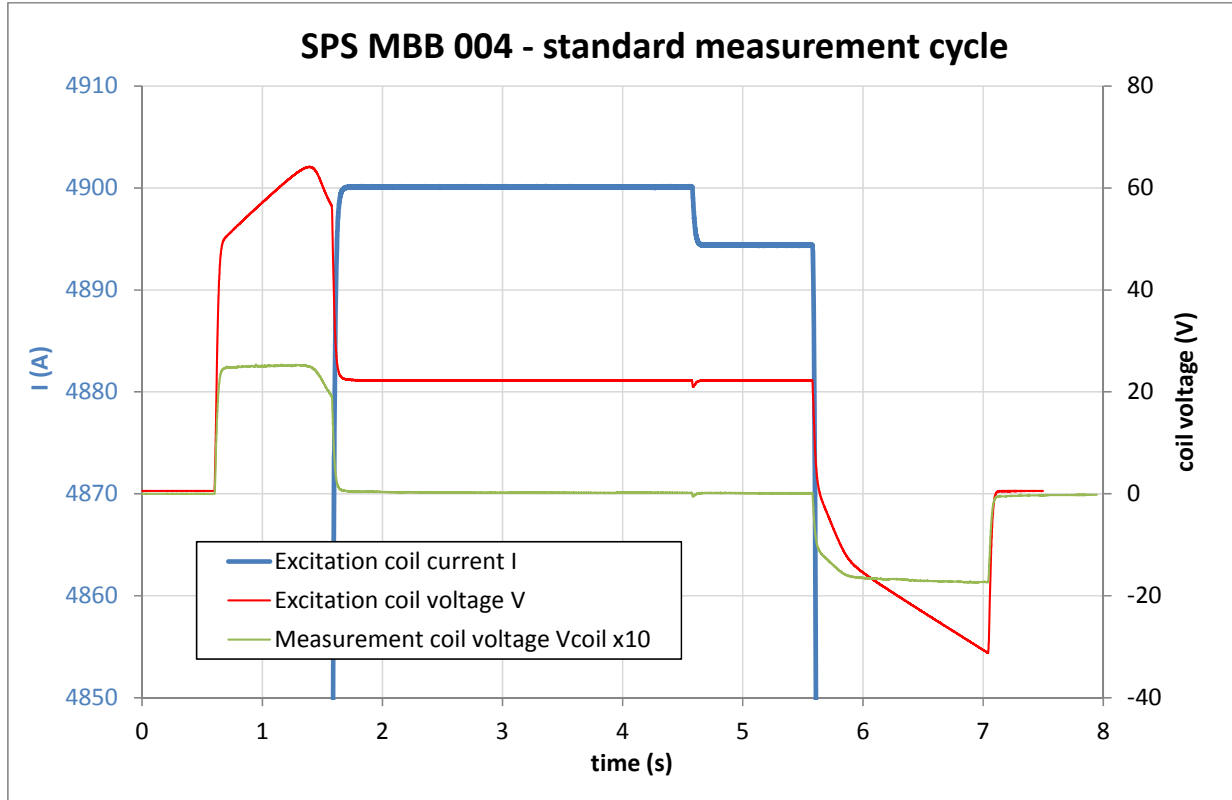


Fig. 9 – Zoomed-in detail from Fig. 8 (downward step in the excitation current at  $t=4.6$  s)

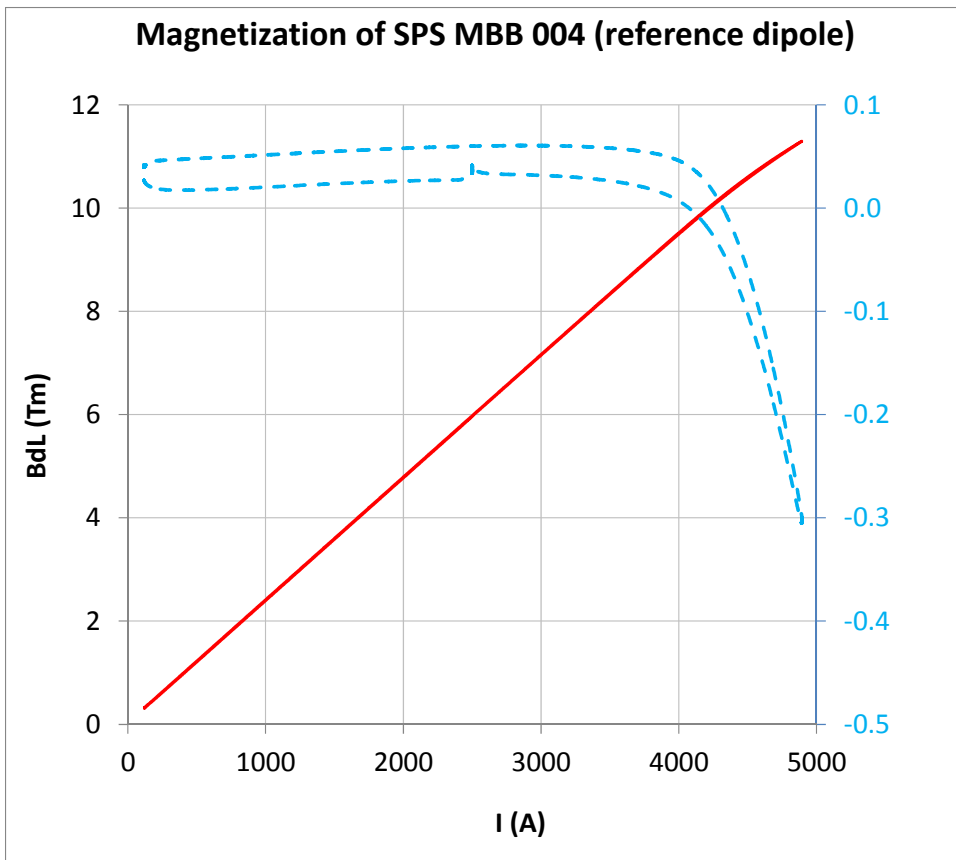


Fig. 10 – Integral magnetization curve  $BdL(I)$ . The difference between the two branches of the hysteresis curve is dashed in blue (same units of Tm, right vertical axis)

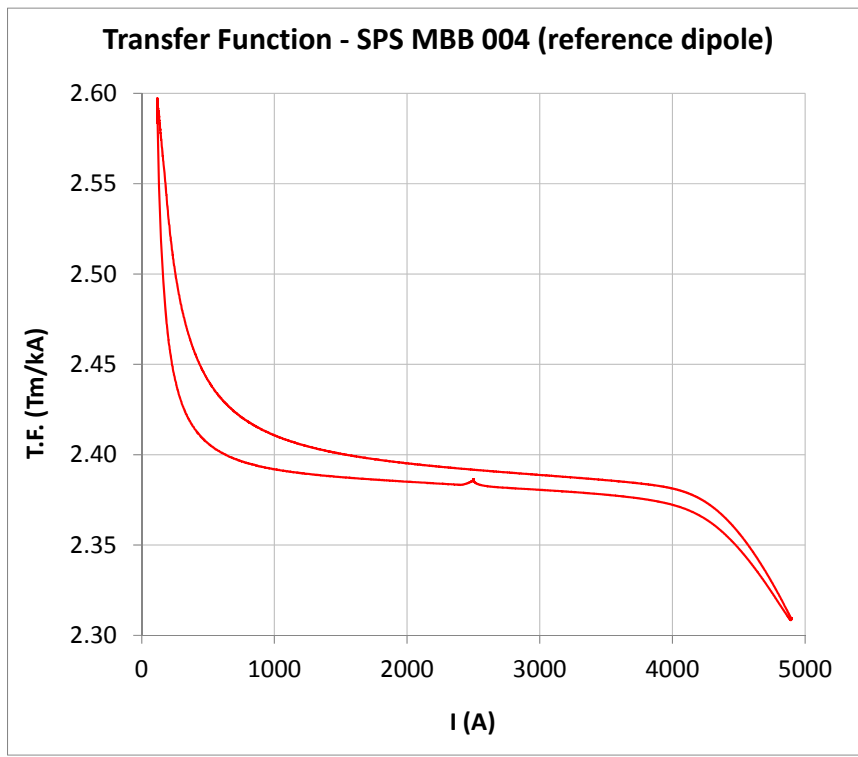


Fig. 11 – Integral transfer function curve  $BdL(I)/I$

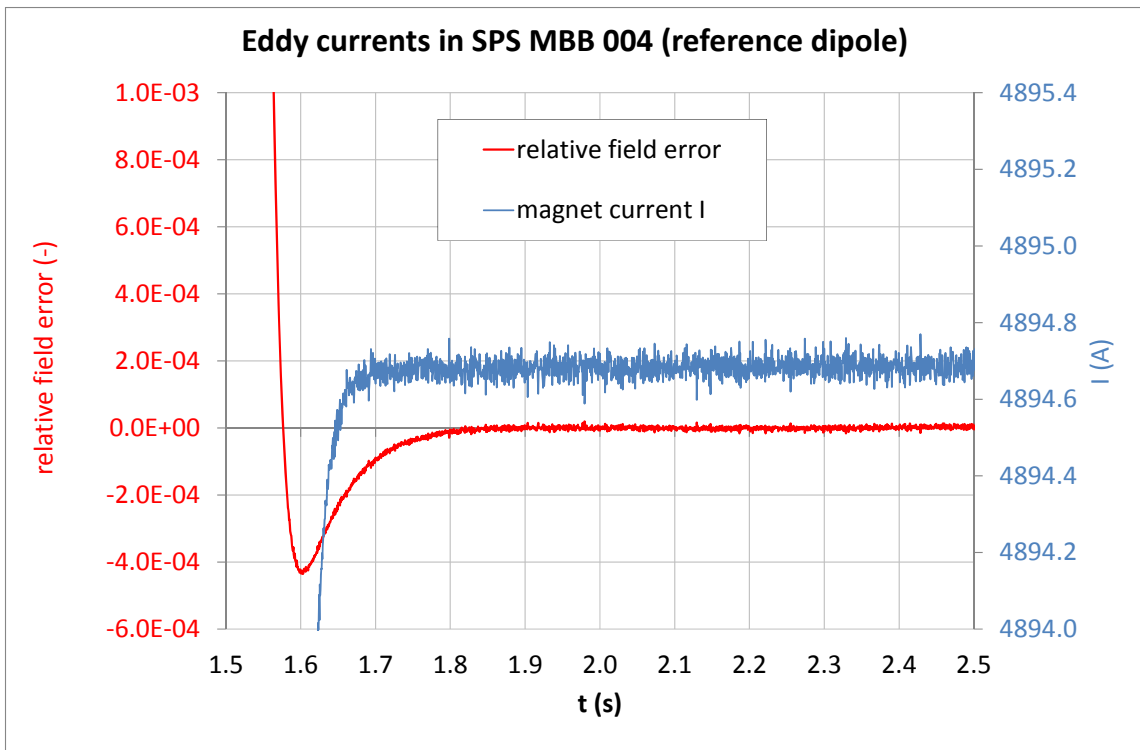


Fig. 12 – Magnetic field behavior at the end of the ramp-up, showing the exponential decay of the eddy currents  
 relative field error = (integral field normalized to  $I(4.5)/I(t)-1$ )

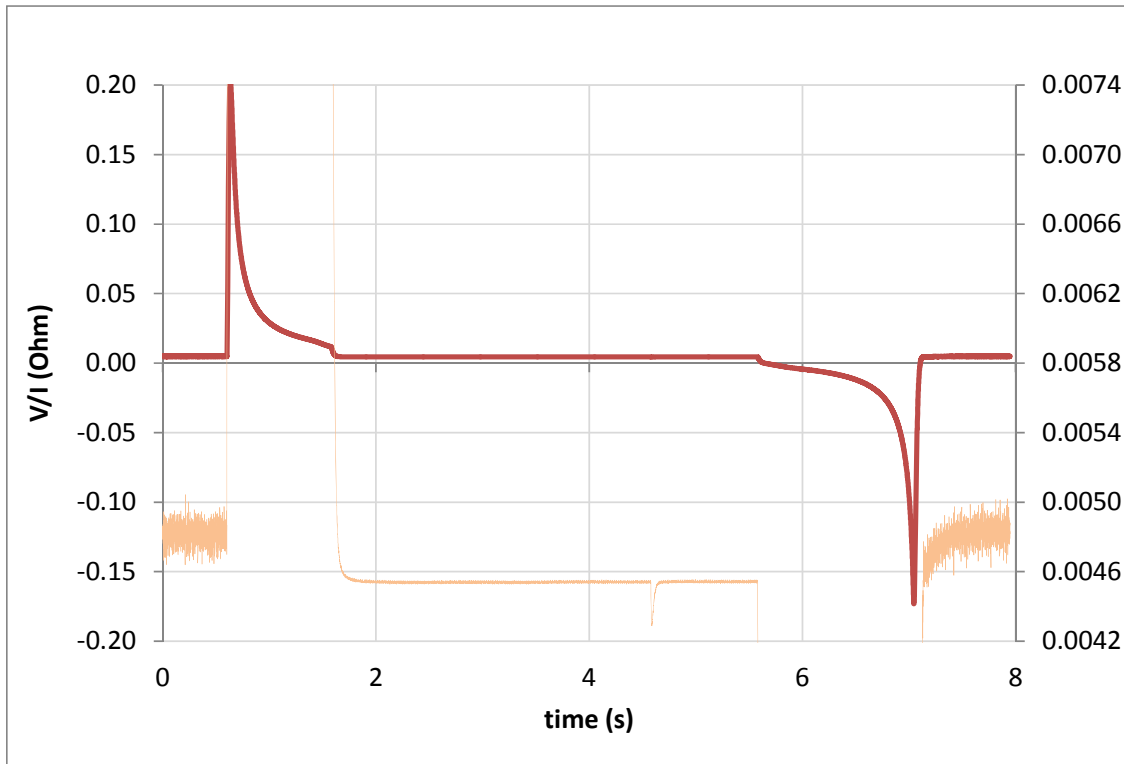


Fig. 13 –  $-V/I$  curve for the calculation of the excitation coil resistance (in orange the same curve on a magnified scale)

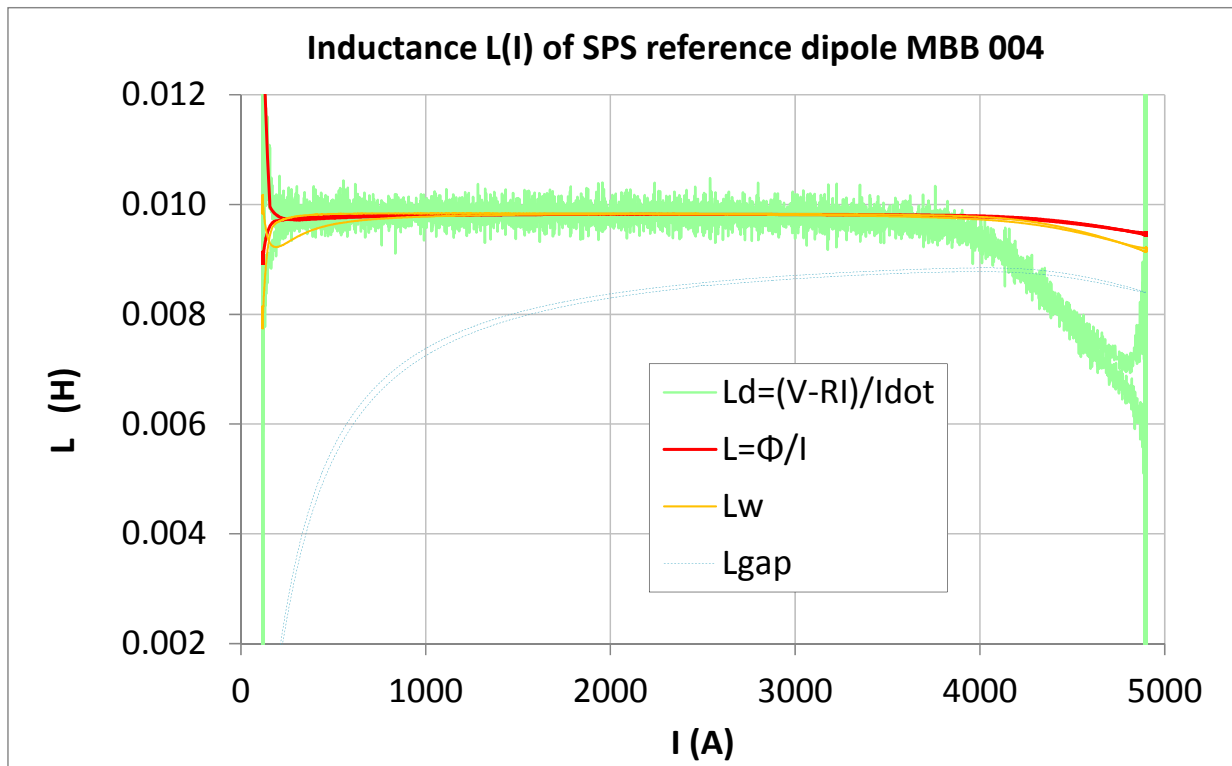


Fig. 14 – Comparative plot of the apparent, differential, energy equivalent and gap inductances  
 (to be compared to Fig. 5)

## 6 Conclusions

We have revised the various definitions of the inductance of a magnet and clarified their relationship, focusing on the deviation from linearity  $\Delta L$  due to iron saturation at high field. In particular we have considered the differential inductance  $L_d$ , which is the parameter of interest in the context of controlling precisely the excitation current.

A large drop of the differential inductance at saturation is to be expected even for magnets which would appear, judging by magnetization measurements, to be affected only mildly. In the case of SPS main dipoles of type MBB, for instance, a magnetic field saturation of just 3.4% corresponds to a differential inductance saturation of almost 40%.

Measurement of the inductance curves can be done when necessary on the test bench in parallel with standard magnetic tests, adding little cost to the test program. High sampling rate of the excitation current and voltage signals is essential to reduce errors due to the noise inherent in  $L_d(I)$ .

In case such measurement is not possible, the drop of differential inductance may be predicted from the magnetic field behaviour using (9), (28) and (31), at the cost of additional uncertainty due to the leaking flux fractions  $\lambda_{coil}$  and  $\lambda_{yoke}$ . These should be then estimated independently, for example via 3D finite element analysis or from accumulated statistical knowledge on similar magnets.

## References

- [1] L. T. Rader, E. C. Litscher, "Some Aspects of Inductance When Iron is Present", AIEE Trans. vol. 63, p.133, 1944
- [2] L.D. Landau, E. M. Lifshitz, Electrodynamics of continuous media, Pergamon Press, 1984
- [3] S. Russenschuck, Field Computation for Accelerator Magnets : Analytical and Numerical Methods for Electromagnetic Design and Optimization, Wiley, 2010
- [4] J.R. Brauer, Magnetic actuators and sensors, Wiley, 2006
- [5] A.D. Polyanin, V.F. Zaitsev, Handbook of exact solution for ordinary differential equations, CRC Press, 1995

## Acknowledgement

The authors wish to acknowledge J. Bauche and G. le Godec for motivating this analysis and providing essential data.

Thanks to S. Russenschuck, D. Tommasini, E. Todesco, and L. Walckiers for helpful discussions and suggestions.